LHCb Collaboration LHCb 2002-039 VELO
28th June 2002

Performance of a wide pitch n–on–n silicon detector with floating strips

M. Charles [1], P. Collins [2], H. Dijkstra [2], O. Dormond [3], M. Ferro-Luzzi [2], R. Frei [3], G. Gagliardi [3], L. Kappert [4], T. Ketel [4], S. Klous [4], J. Libby [2], D. Malinow [5], K. Österberg [2 6], J.P. Palacios [7], C. Parkes [7 8], U. Parzefall [2], T. Ruf [2], P. Sizun [9], F. Teubert [2], M. Witek [10]

Abstract

First measurements of charge sharing and collection for a 95 μm pitch n–on–n silicon sensor with floating strips are presented. These measurements were made with an analogue front–end sampling at 40 MHz. The charge collection performance is compared to a region of the detector where the strips are bonded consecutively. Strips with a significant signal are found to be correlated with opposite polarity signals in the strips neighbouring them. This phenomenon is described and compared to measurements with alternative silicon sensors and electronics.

[1]Department of Nuclear and Particle Physics, Oxford University, 1 Keble Road, Oxford OX1 3RH, England
[2]CERN, CH-1211, Geneva 23, Switzerland
[3]Institut de Physique des Hautes Energies, Batiment des Sciences Physiques, Université de Lausanne, CH-1015 Dorigny 20, Switzerland
[4]NIKHEF, Kruislaan 409, 1098 SJ Amsterdam, The Netherlands
[5]University of Maryland, College Park MD 20742, USA
[6]Now at Helsinki Institute of Physics (HIP), University of Helsinki, Faculty of Science, P.O. Box 64 (Gustaf Hällströmin katu 2), 00014 University of Helsinki, Finland.
[7]University of Liverpool, Oliver Lodge Laboratory, Liverpool, England
[8]Now at University of Glasgow, Department of Physics, Glasgow G12 8QQ, UK.
[9]E.N.S.M.P., Paris, France
[10]Institute of Nuclear Physics High Energy Departments, ul. Kawiory 26 A, 30-055 Kraków, Poland

1 Introduction

The outer region of the 'ultimate ϕ–sensor', described in the VELO Technical Design Report [1], has one floating strip between those strips read out. Charge collected on the floating strip is shared between its two neighbours; calculating the cluster centre from the two strips leads to an improved ϕ–measurement. The advantage of using floating strips is that the enhanced precision comes with no increase in the number of electronics channels.

The LHCb VELO test–beam group has measured the performance of floating strips on a detector with n^+–side segmentation at a sampling rate of 40 MHz; these are the silicon technology and readout rate requirements for the LHCb VELO. These are the first measurements of the charge sharing and collection as a function of the track position with such a wide pitch n–on–n detector equipped with electronics sampling at 40 MHz.[1] This note describes the results of these measurements which were made at the CERN SPS using a beam of 120 GeV muons and pions. The note begins with a description of the detector and electronics used in Section 2; this is followed by an outline of the test–beam set–up used to study the detector in Section 3. The data are described in Section 4, along with the alignment results and the track selection applied. The charge sharing and charge collection performance is given in Section 5, which includes also a discussion of correlated signals of opposite polarity observed in channels adjacent to a strip with significant signals. These results are then discussed, and conclusions given, in Section 6.

2 Detector description

The detector evaluated is a double–sided micro–strip detector manufactured by Canberra.[2] The detector is a prototype for the strip layer of the Inner Tracking System of the ALICE experiment [3]. Figure 1 is a schematic of the n–side of the sensor. The detector has 128 strips with a pitch of 95 μm. Each strip has a 1° stereo angle, the sense of which is shown in Figure 1. The n^+–strips are isolated from one another by p^+–doped regions. The detector is 300 μm thick. The high voltage is applied to the detector strips using Field OXide FET (FOXFET) biasing [4].

The detector was bonded to a hybrid carrier equipped with three SCT128A ASICs (Application Specific Integrated Circuits) [5]. The SCT128A is an analogue–pipeline front–end ASIC capable of sampling 128 channels at 40 MHz. Due to the different pitches of the hybrid and the detector two SCT128A ASICs were required to bond all the strips; the majority of SCT128A channels were unconnected. Twenty consecutive strips were bonded to the hybrid; the remaining strips were bonded alternately, with a floating strip in between. The regions of consecutively bonded and floating strips are indicated in Figure 1.

3 Test–beam set–up

The detector was operated in a 120 GeV beam of muons and pions at the CERN SPS along with a beam–telescope; the telescope is described elsewhere [6]. The track extrapolation

[1] Measurements of the signal from a floating strip double–sided detector, with a pitch of 37.5 μm and two intermediate strips read out with 75 ns shaping time deconvolution electronics, have been made [2].

[2] Canberra Semiconductors N.V., Lammerdries 25, 2259 Olen, Belgium.

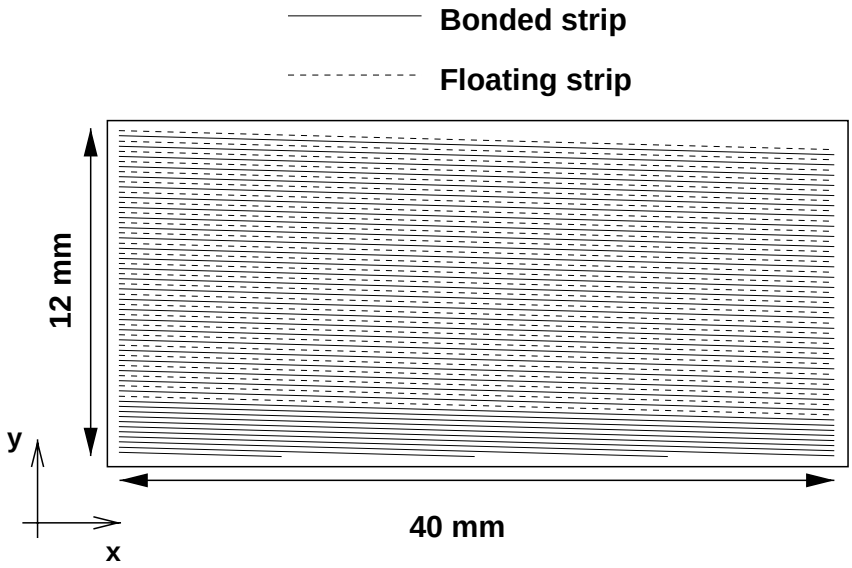

Figure 1: A schematic of the n–side of the test detector. The bonded (solid) and floating (dashed) strips are shown.

Run number	Bias voltage (V)	Triggers	Reconstructed tracks	Tracks passing selection
4356–4411	70	133511	90764	7526
4692–4709	100	89907	54605	3355

Table 1: The data sample used in the analysis. The track selection and analysis cuts are described in the text.

precision was estimated to be 24 μm at the position of the ALICE detector.

The test detector data were sampled at 40 MHz. The readout was triggered by coincidence between two or four scintillators in the beam–line.[3] A TDC (Time–to–Digital Converter) was used to record the relative time between the beam–trigger and the sampling of the SCT128A. A single pipeline location was readout with each trigger. A veto was applied to the trigger while the beam–telescope and test detector data were read out, digitised and stored to disk [6].

4 Data sample

The data collected with the test–detector are summarised in Table 1. The principal results presented in this note are for the sample taken at a bias voltage of 100 V, though checks were made with the other sample. With FOXFET, or punch through biasing, the voltage on the strips is 10 to 20 V lower than that applied; the detector depletes at between 40 to 60 V [3]. The track reconstruction, telescope alignment and track selection are discussed below.

[3]If two scintillators were used a smaller fiducial volume was defined.

Fiducial cuts on track intercept with telescope stations in local coordinates
$\lvert\phi\rvert < 0.58$ radians $R > 1.1$ cm AND $R < 3.5$ cm $R < 2.76$ cm OR $R > 2.86$ cm $\lvert R\phi\rvert > 0.05$ cm
Cuts on residuals ($d_{\rm res}$) between track intercept and the cluster on the track
R–sensor: $\lvert d_{\rm res}\rvert < 0.0016$ cm ϕ–sensor: $\lvert d_{\rm res}\rvert < 0.004$ cm
Cuts on pull ($d_{\rm res}/\sigma_{d_{\rm res}}$) between track intercept and the cluster on the track
$\lvert d_{\rm res}/\sigma_{d_{\rm res}}\rvert < 0.8$ or 1.6 (depends on position in telescope)
Cuts on the stereo–pull for ϕ–sensors between track intercept and the cluster on the track
$\lvert$stereo pull$\rvert < 0.8$ or 1.6 (depends on position in telescope)

Table 2: The track selection criteria. If a track fulfilled these criteria it was selected. A looser cut on the pulls was applied to the central telescope detectors which have a wider distribution than the stations at the ends.

4.1 Track reconstruction and alignment

The raw data of the detectors were processed with pedestal subtraction and common–mode noise suppression algorithms. Hit strips were identified on the detectors and were used to form clusters with adjacent strips. Tracks were then fitted through the clusters on the beam–telescope detectors [7].

The alignment of the telescope was performed using tracks passing the selection described below. This improved the internal alignment of the telescope and the test detector. The alignment of the telescope was performed by minimising the χ^2 of the distance between the tracks' intercepts to the cluster positions on the detector.

The residuals on the test–detector are shown as a function of x and y in the local coordinate scheme of the test–detector in Figure 2(a) and (b), respectively. The Cartesian coordinate system is indicated in Figure 1. The residual distribution is given in Figure 3; the fitted Gaussian width of the distribution is 50 μm.

The mean residual distributions as a function of local position show deviations from zero at the 10 to 20 μm level. These deviations are indicative of problems in the internal alignment of the R and ϕ sensors of the telescope.[4] The deviations are small compared with the 95 or 190 μm pitch of the connected strips.

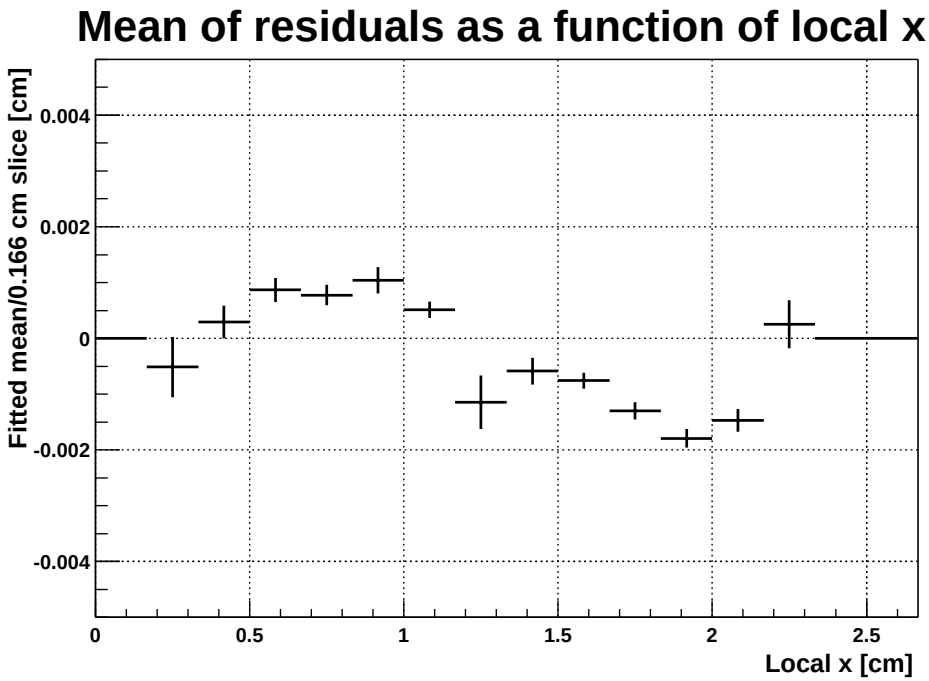

(a)

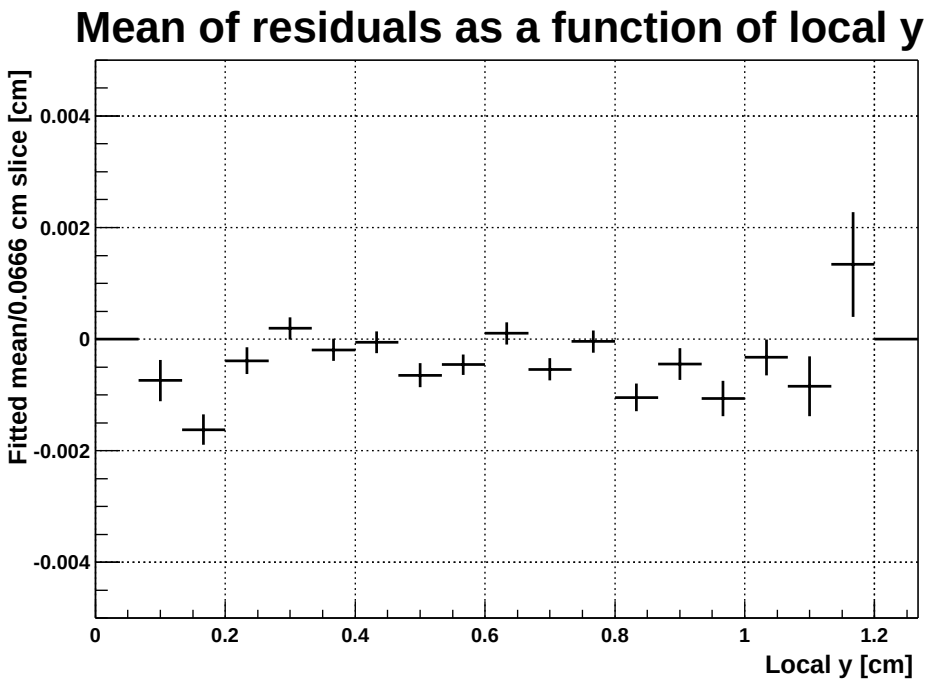

(b)

Figure 2: The mean of the fitted residual distributions as a function of (a) local x and (b) local y, corresponding to the x and y of Figure 1.

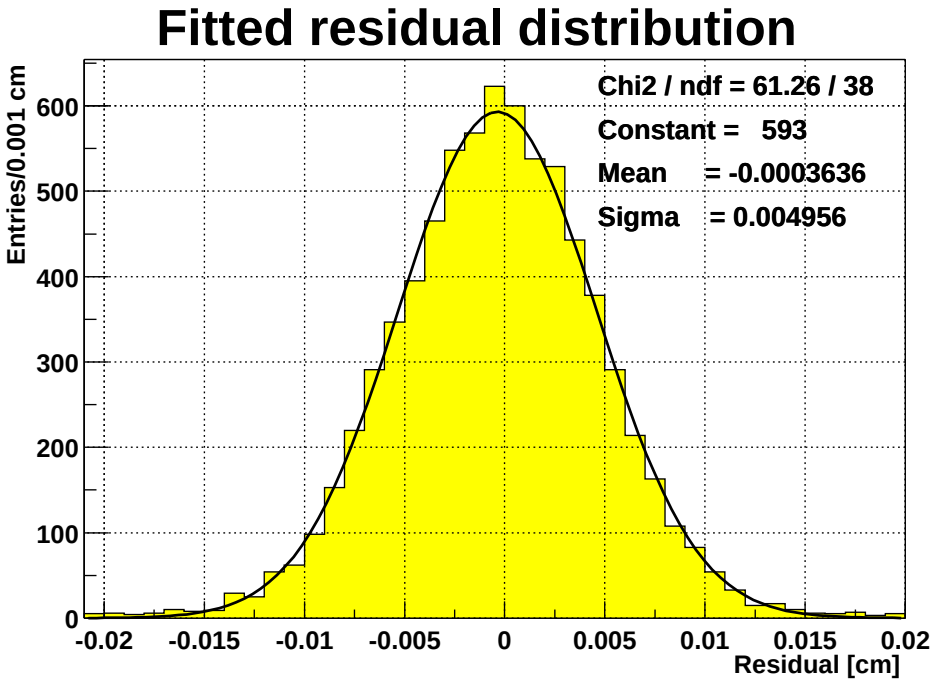

Figure 3: The fitted residual distribution.

4.2 Track selection

The cuts applied to the tracks used in the analysis are listed in Table 2. A detailed description of the telescope detector's geometry can be found in [8]. The fiducial cuts ensured that the clusters used to reconstruct a track were well contained within the sensitive area of the beam–telescope detectors. The cuts placed on the absolute value and pull of the residuals between the track intercept and the cluster centre were to remove outliers; this requirement improved the alignment of the beam–telescope. The cluster error parameterisation used to construct the pull is pitch dependent and taken from [9].

The non–zero stereo angle in the ϕ–measuring sensors allows a measurement of R (R_ϕ) as well as a pseudo–ϕ. The *stereo–pull* is defined as the residual between R_ϕ and the R of the track intercept on the sensor, divided by the associated error. The definition of the R_ϕ–measurement is shown schematically in Figure 4. Examples of the R_ϕ–residual and of its stereo–pull for one of the beam–telescope ϕ–sensors are shown in Figure 5. The RMS of the R_ϕ–residual distribution and the stereo–pull distribution are 189 μm and 1.01, respectively.

The trigger used in the test–beam was asynchronous with the SCT128A sampling. Therefore, reconstructed tracks in the telescope detectors, which were read out using VA2 electronics with a shaping time of the $\mathcal{O}(\mu s)$ [10], could be out–of–time with signals in the SCT128A which has a shaping time of the $\mathcal{O}(25$ ns). The TDC time was used to reject out–of–time tracks. Figure 6 shows the integrated signal on the two strips about the intercept point of a track on the test detector as a function of TDC–time. The signal–shape from the SCT128A can be seen clearly, and has a maximum at around 15 ns. Tracks

[4]Before the implementation of the track selection, described in Section 4.2, the maximum deviation in the mean position was greater than 40 μm.

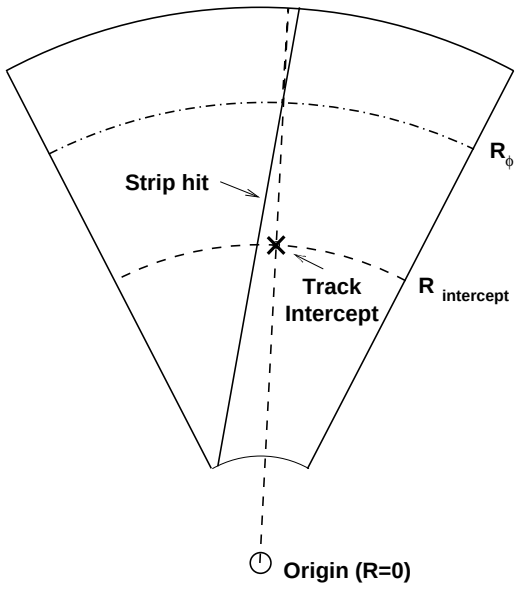

Figure 4: A schematic of the R_ϕ–measurement, using the stereo angle of the ϕ–strips. The stereo residual is R_ϕ - $R_{\text{intercept}}$. All coordinates (R, ϕ) are in the local frame of the detector.

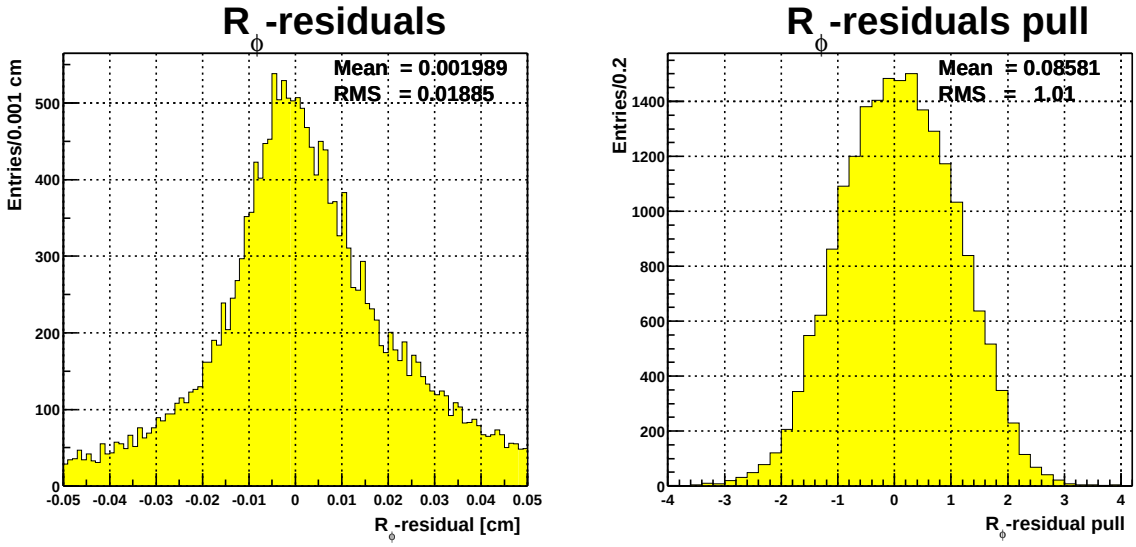

Figure 5: The (left) R_ϕ residuals and (right) the stereo–pull for one of the ϕ–measuring telescope sensors.

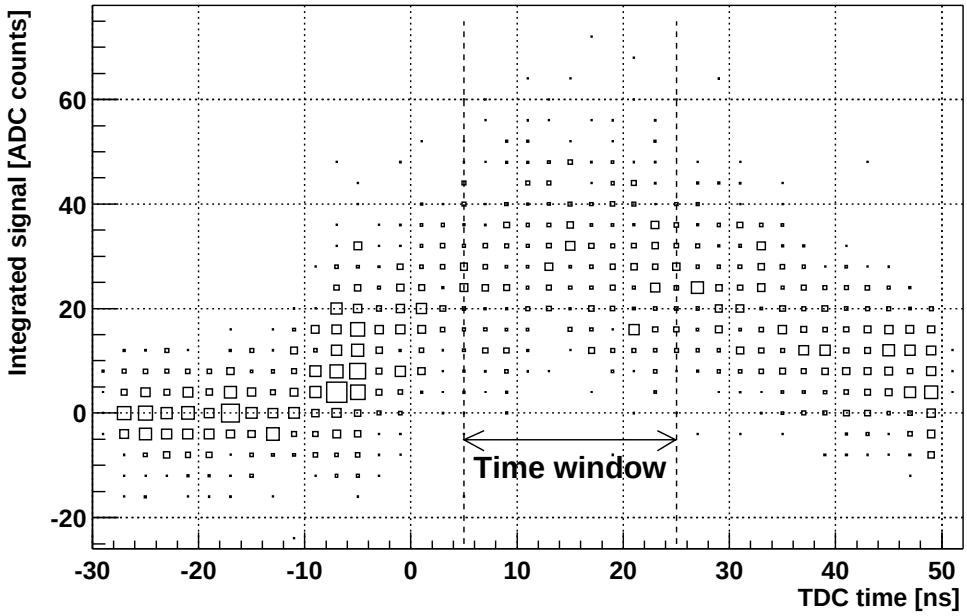

Figure 6: The sum of the signal on the two strips adjacent to the intercept point on the test detector as a function of the TDC time. The TDC time has an arbitrary offset. Events in the time window indicated were used in the analysis.

within the time interval 5 to 25 ns were considered to be in–time and were used in the analysis.

The 20 ns window about the peak leads to few events having the optimum signal; however, too restrictive a selection would significantly reduce the statistics available for the analysis. Therefore, the use of a time window leads to a reduction in the signal measured. This reduction was estimated to be around 7% for a uniform time distribution convoluted with the SCT128A signal–shape [11].

5 The performance of the floating–strips

The two measurements discussed in Section 5.1 and Section 5.2 are the charge sharing and the charge collection performance with floating strips, respectively. In Section 5.3 the floating strip performance is compared to that of the region with consecutively bonded channels. The results for opposite polarity signals in the neighbouring strips to the intercepted strip are presented in Section 5.4. Finally, in Section 5.5, other measurements of the signal in neighbouring strips for different detectors, bonding or electronics are presented.

5.1 Charge sharing

The charge sharing was studied by reconstructing the value of η:

$$\eta = \frac{Q_{\mathrm{Left}}}{Q_{\mathrm{Left}} + Q_{\mathrm{Right}}} \ ,$$

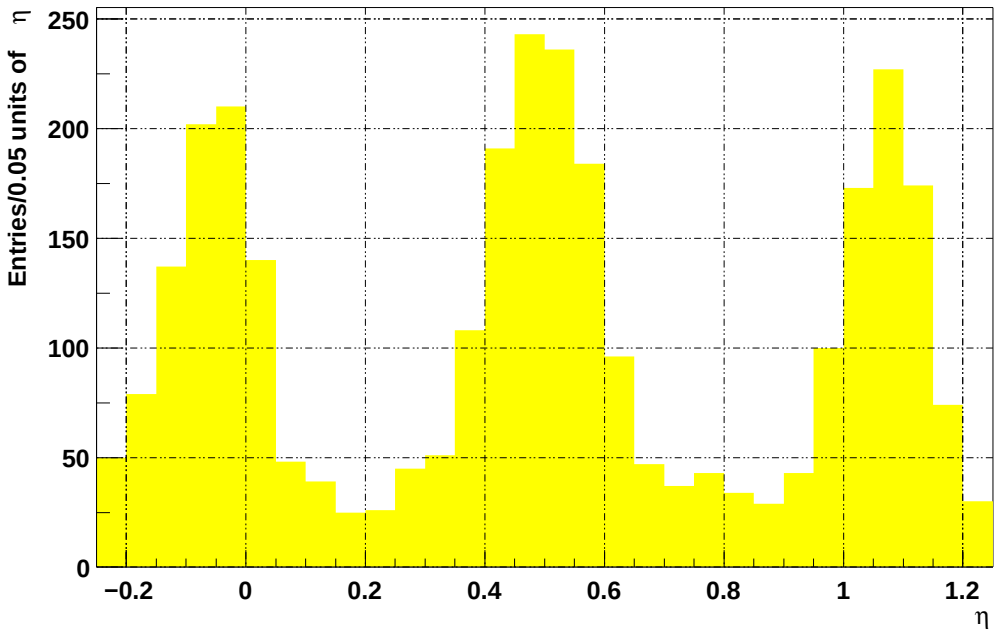

Figure 7: The reconstructed value of η for tracks intercepting the region of the test–detector with floating strips.

where Q_{Left} (Q_{Right}) is the signal on the strip to the left (right) of the intercept point of a track with the test detector. Left is defined to be at a smaller value of y in the local Cartesian coordinates given in Figure 1.

Figure 7 shows the η–distribution for tracks intercepting the region of the test detector bonded with a floating strip between each connected channel. The distribution has three distinct peaks at $\eta \approx 0$, $\eta \approx 0.5$ and $\eta \approx 1$. The peaks at $\eta \approx 0$ and $\eta \approx 1$ correspond to the majority of the charge being collected on the right or left connected strip, respectively. The peak at $\eta \approx 0.5$ arises from the majority of the charge being collected on the floating strip and then divided equally between the two connected strips adjacent to it. This is the desired charge–sharing behaviour for a strip detector with a single floating strip.

The peaks at $\eta \approx 0$ and $\eta \approx 1$ are biased to lower and higher values, respectively. This is due to the opposite polarity signals which are discussed in Section 5.4.

5.2 Charge collection

Figure 8(a) shows the sum of Q_{Left} and Q_{Right} as a function of the value of η. Projections in $|\Delta\eta| = 0.1$ intervals were fitted with a Landau function and the most probable value of the fitted distributions are given in Figure 8(b). The Landau function used is described in [11].

The integrated signal around $\eta \approx 0.5$ is approximately 60% of the signal at $\eta \approx 1$ and $\eta \approx 0$. The decrease in signal where the charge read out was collected on the floating strip is expected. The charge read out is capacitively coupled to the neighbouring strips. However, some charge is capacitively coupled to the detector backplane which is not collected. The ratio between the signal collected on a floating strip (s_f) to a connected

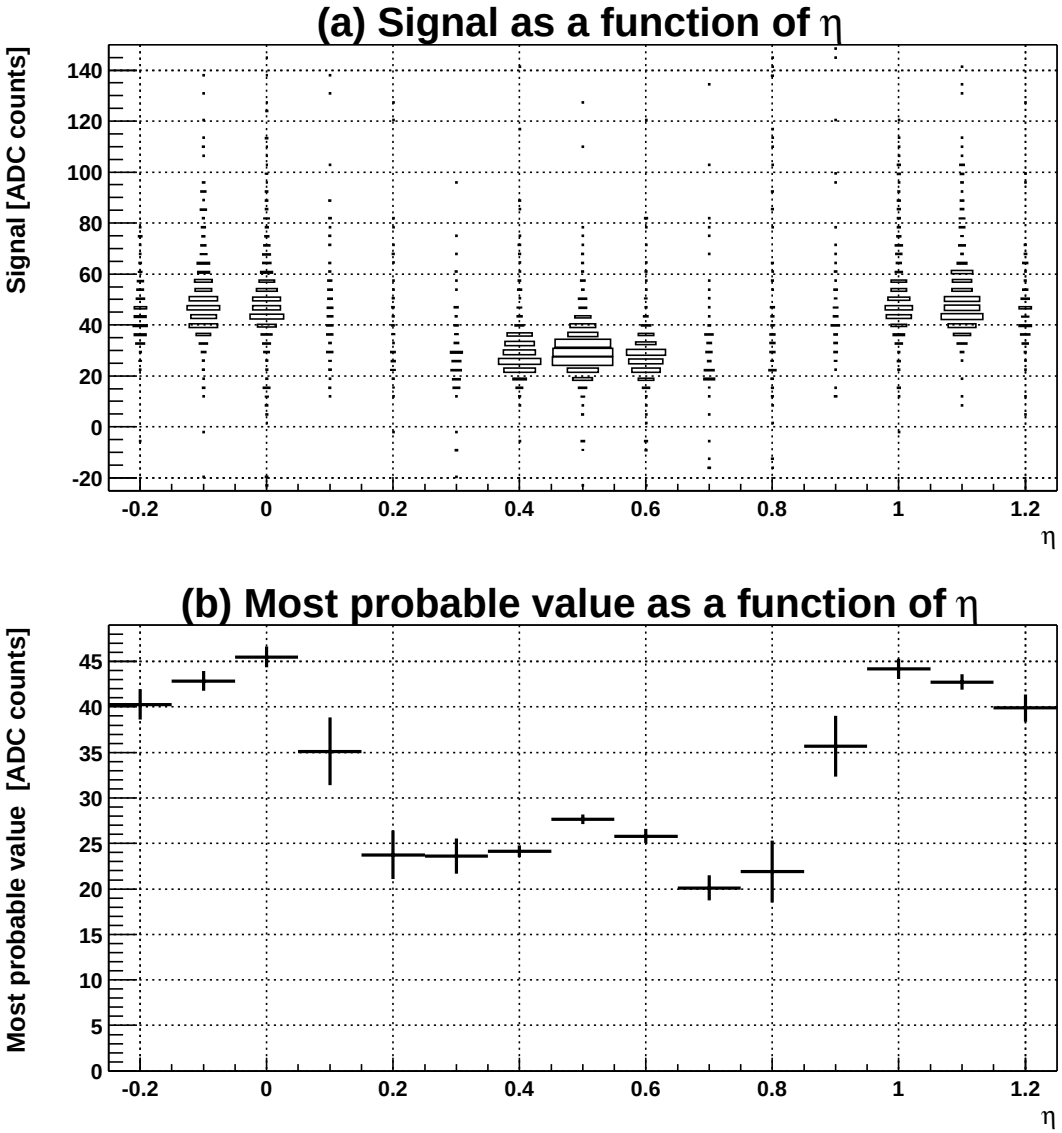

Figure 8: (a) The signal ($Q_{\rm left} + Q_{\rm right}$) collected as a function of η and (b) the most probable value of a Landau function fitted to each $|\Delta\eta| = 0.1$ interval, for tracks intercepting the region of the test–detector with floating strips.

strip (s_c) obeys the relation:

$$\frac{s_f}{s_c} = \frac{4C_{n1}C_c}{C_b(C_{n1}+C_c)+4C_{n1}C_c} \ ,$$

where C_{n1} is the inter–implant capacitance, C_c the coupling capacitance to the aluminium readout lines and C_b is the strip–backplane capacitance [12]. Using the measured values of s_f and s_c combined with the condition that $\frac{C_c}{C_{n1}} \geq 20$ [3] leads to the constraint:

$$2.6 \leq \frac{C_b}{C_{n1}} \leq 2.7 \ ,$$

on the ratio between the strip–backplane capacitance to inter–implant capacitance. This ratio would need to be reduced to improve the charge collection on the intermediate strip.

Figure 9(a) shows the sum of Q_{Left} and Q_{Right} as a function of the value of the distance from the left–hand connected strip. Projections in $|\text{strip}| = 0.1$ intervals were fitted with a Landau function and the most probable value of the fitted distributions are given in Figure 9(b). The signal is seen to decrease away from a distance of 0 or 1; the region around 0.5 corresponds to the implant of of the floating strip. No signal loss is seen between strips at a distance of 0.25 and 0.75 of a strip, which corresponds to the mid–points between strip–implants.

The largest most probable values, measured when $\eta \approx 0$ and $\eta \approx 1$, are 45 ADC counts in Figure 8(a); when corrected for the sampling over a 20 ns window this gives a peak signal of 48 ± 1 ADC counts. This is 15% lower than the signal measured with a different 300 μm thick detector readout with identical electronics [11]. The difference could be related to gain variations of the SCT128A ASICs used. However, only 5 to 10% differences were measured on functional SCT128A ASICs in the laboratory; these SCT128A ASICs were from the same wafers as those used for the test–detector [13].

5.3 Consecutively bonded strip performance

Figure 10(a) shows the value of η reconstructed for tracks intercepting the region of the detector with consecutively bonded strips, thus no floating strips. Peaks at $\eta = 0$ and $\eta = 1$ can be seen, these correspond to the majority of the charge being collected on the right–hand or left–hand strip, respectively. For this pitch, significant charge sharing is not expected. The number of events with tracks intercepting the consecutively bonded strip region was only 96 after the full selection. Figure 10(b) shows the value of η reconstructed for tracks intercepting the region of the detector with consecutively bonded strips when the track selection described in Table 2 was not applied; the event was required to pass the TDC time selection. The statistics are greatly increased and no evidence for any significant charge sharing in the consecutively bonded strips region can be seen.

The sample with only a timing selection applied was used to extract the total signal. For the peaks around $\eta = 0$ and $\eta = 1$ the most probable value of the signal was 53 ± 2 ADC counts where the error is statistical; the correction for sampling over a 20 ns time–window has been applied. The most probable value of the signal is slightly higher, though in reasonable agreement, with that found for the floating strip region when the majority of the charge is collected on a bonded strip. The value is in better agreement with previous measurements with a 300 μm thick detector [11].

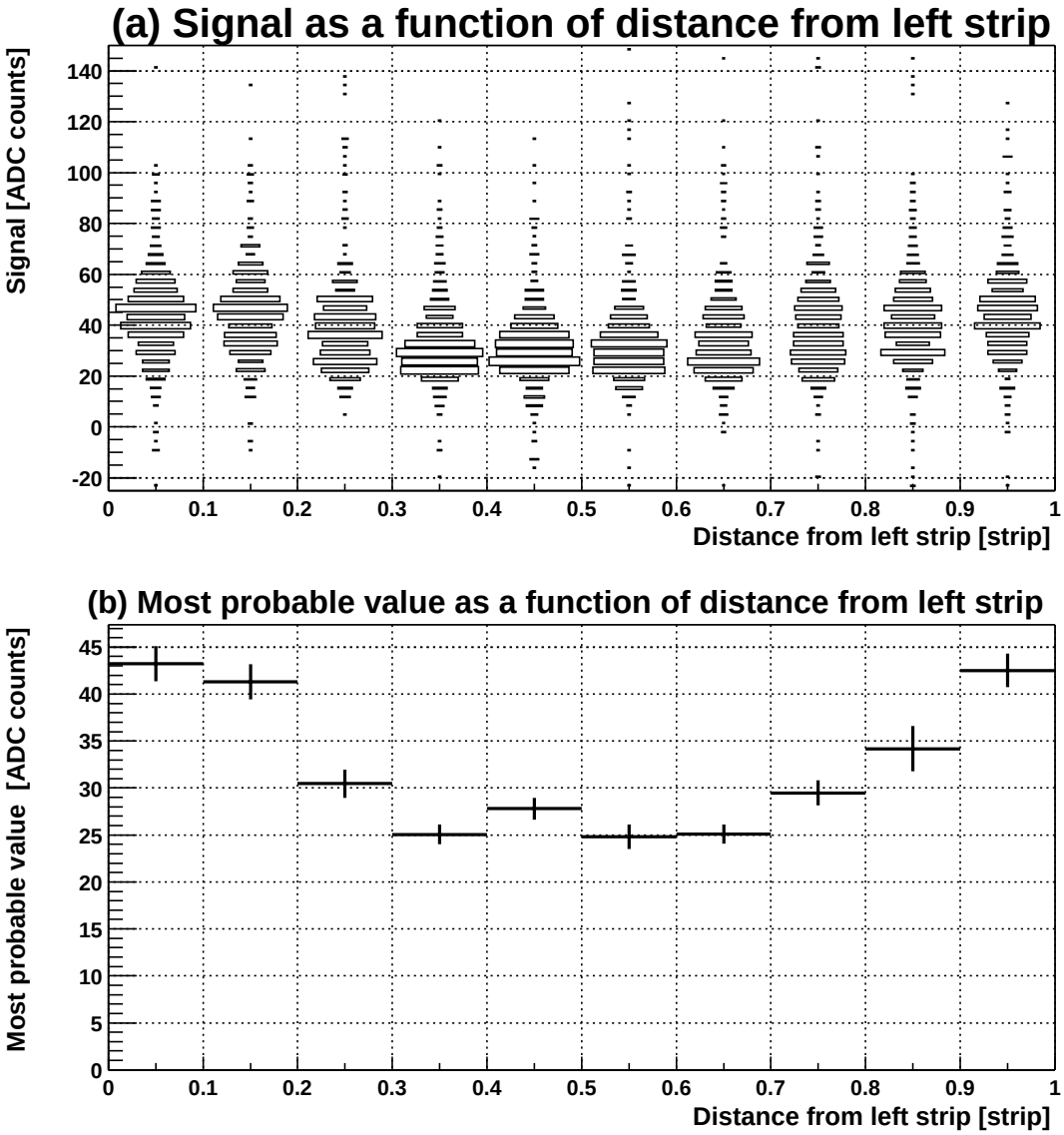

Figure 9: (a) The signal ($Q_{\rm left} + Q_{\rm right}$) collected as a function of the distance from the left–hand connected strip and (b) the most probable value of a Landau function fitted to each |strip| = 0.1 interval, for tracks intercepting the region of the test–detector with floating strips.

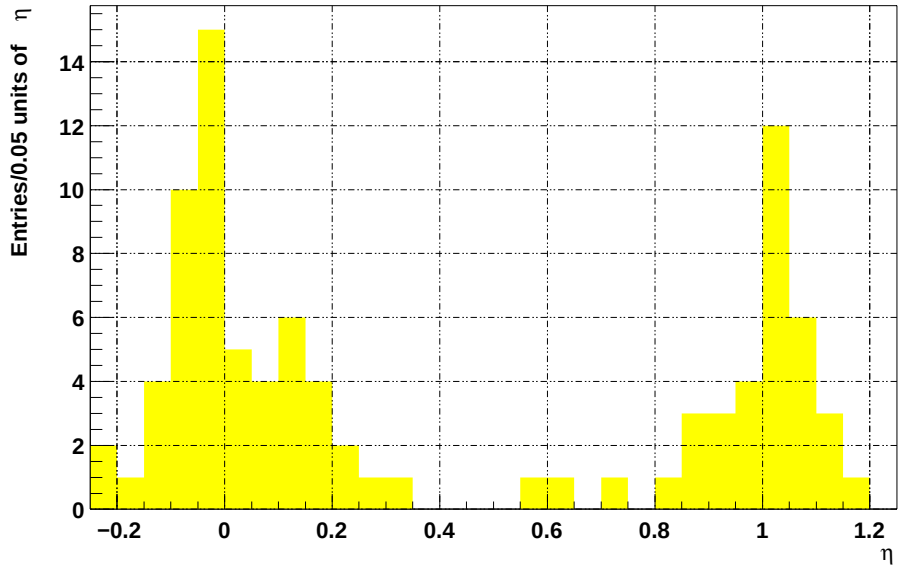

(a)

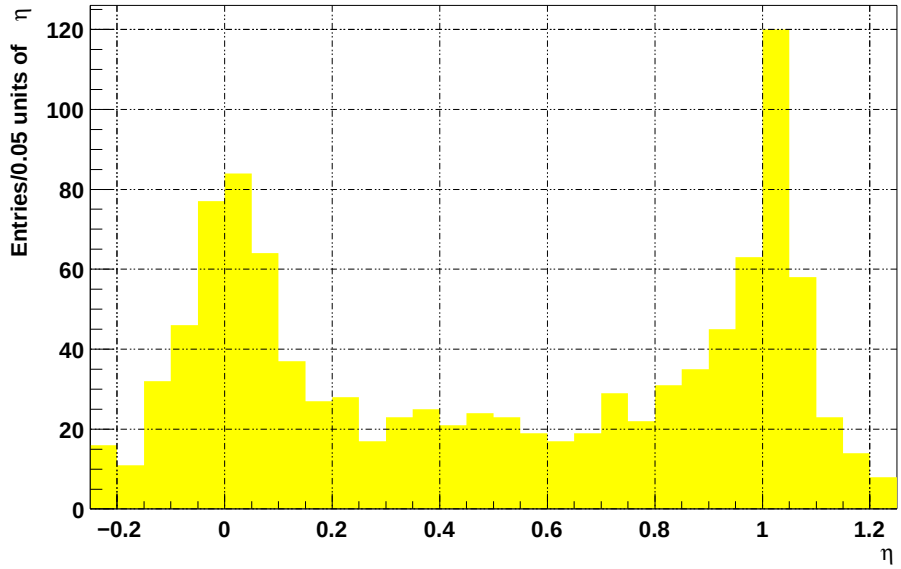

(b)

Figure 10: The reconstructed value of η for tracks intercepting the region of the test–detector with consecutively bonded strips (a) with and (b) without track selection.

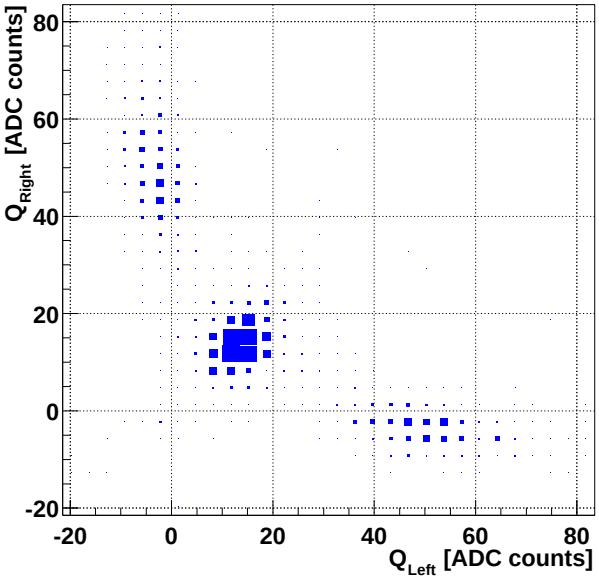

Figure 11: Q_{Left} and Q_{Right} plotted against one another for tracks intercepting the region of the detector bonded with floating strips.

5.4 Opposite polarity signals in neighbouring strips

As noted in Section 5.1 the peaks in the η distribution, where the majority of the charge was collected on a bonded channel are slightly displaced to lower and higher values for $\eta \approx 0$ and $\eta \approx 1$, respectively. Figure 11 shows Q_{Left} and Q_{Right} plotted against one another for tracks intercepting the region of the detector bonded with floating strips. Figure 11 has three regions with significant population:

- large positive Q_{Left} and small negative Q_{Right},
- around $Q_{\mathrm{Left}} \approx Q_{\mathrm{Right}} \approx 15$ ADC counts and,
- large positive Q_{Right} and small negative Q_{Left}.

These regions correspond to $\eta \approx 1$, $\eta \approx 0.5$ and $\eta \approx 0$, respectively.

A significant signal on a strip is correlated with an opposite polarity signal on a connected adjacent strip. Figure 12 shows the ratio of signal on ± 16 nearest–neighbour strips to that on the strip with a significant positive signal (strip 0) for $\eta < 0.1$ or $\eta > 0.9$. The negative signals have a minimum of -6% in the connected strips adjacent to the central strip. The negative signals remain in strips further away, with increasing values, until the signals become positive around the ± 5 strips. Extending out to ± 15 strips the signals remain positive, peaking at $\sim 2\%$ of the signal on the central strip. The integral over the whole range is $1.0 \pm 1.0\%$, thus compatible with zero. The bi–polar signals induced extend over a significant distance of ~ 3 mm.

Figure 13 shows the relative signals on ± 16 neighbouring strips when the charge is collected on a floating strip and then shared between the left and right neighbouring strips. This corresponds to a range of $0.1 < \eta < 0.9$. Opposite polarity signals are observed in

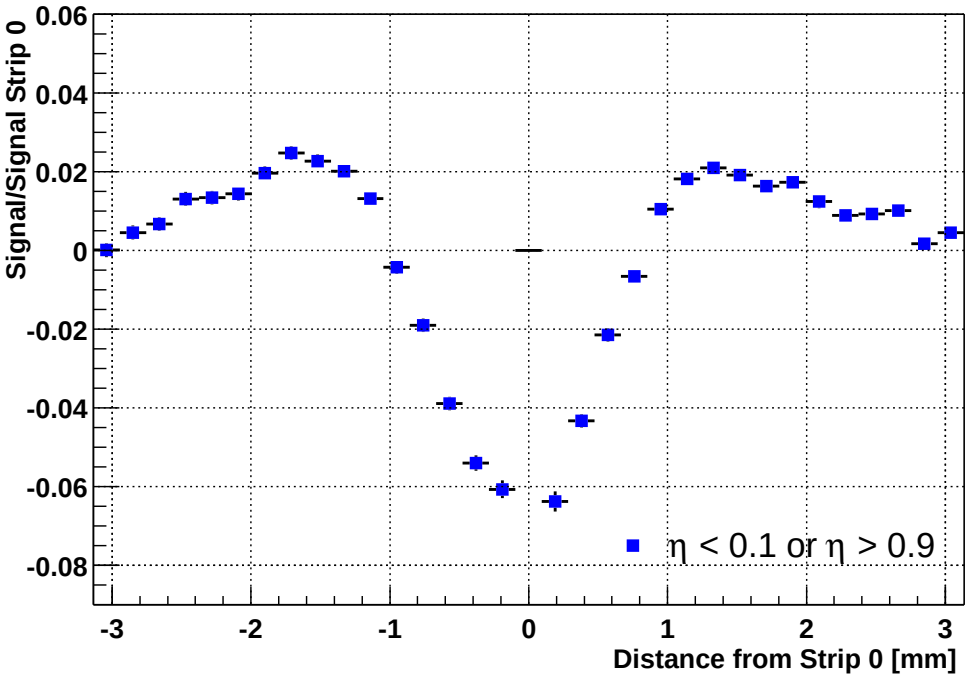

Figure 12: The ratio of signal on ±16 connected nearest–neighbour strips to that on the strip with a significant positive signal (strip 0) for $\eta < 0.1$ or $\eta > 0.9$.

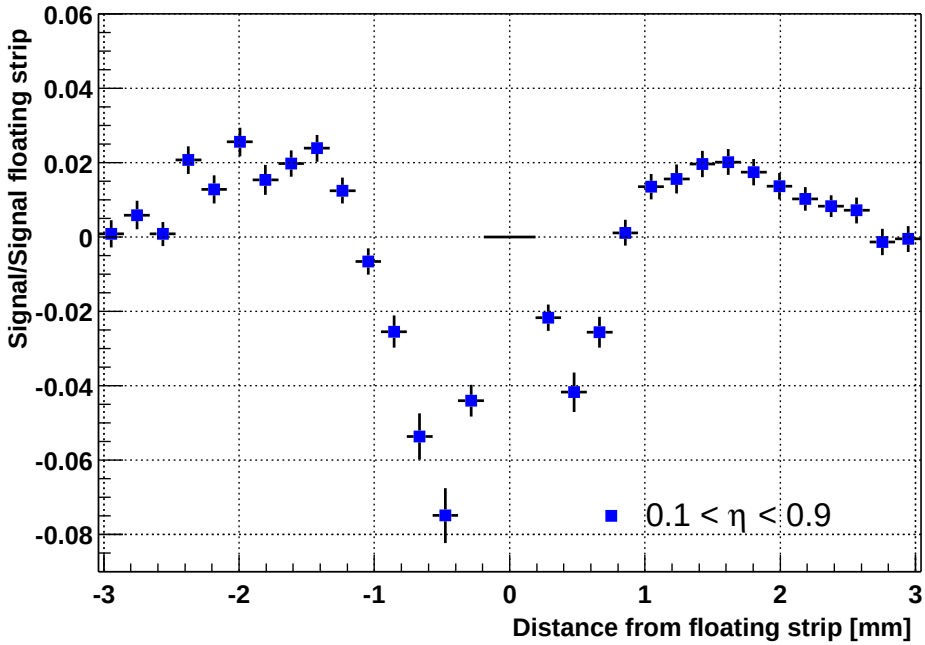

Figure 13: The ratio of signal on ±16 nearest–neighbour strips to that on a floating strip with a significant positive signal which then shares the charge equally to strips left and right. The plot is for $0.1 < \eta < 0.9$.

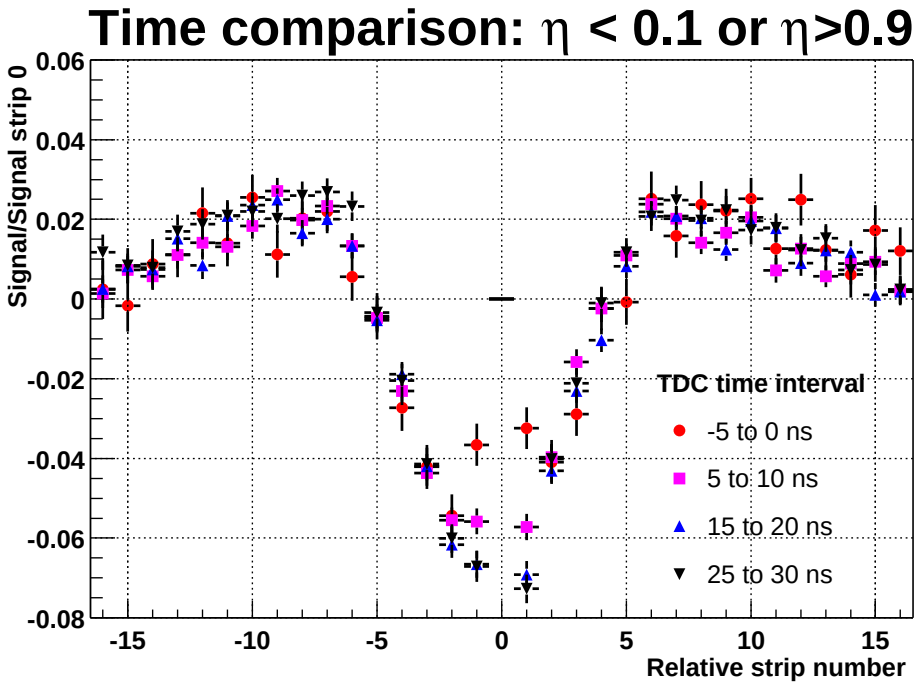

Figure 14: The ratio of signal on ±16 nearest–neighbour strips to that on the strip with a significant positive signal (strip 0) for $\eta < 0.1$ or $\eta > 0.9$ for 4 different time intervals.

neighbouring strips. The relative signal magnitudes are of similar to those for $\eta < 0.1$ or $\eta > 0.9$ given in Figure 12. The shape is slightly distorted but the bi–polar signals when integrated over all neighbouring strips, excluding the ±1 neighbouring strips, gives $-3.1 \pm 2.2\%$ which is compatible with zero.

Cross–checks of the result were performed to ascertain whether the phenomenon was a consequence of an electronics problem. This was done by repeating the measurements separately for each SCT128A, and for events spanning the boundary between the two SCT128A ASICs; in both cases no significant changes to the result were found. The result being a feature of the common–mode correction was also excluded by performing the analysis without the correction. All features of the signal on neighbouring strips remained when no common–mode correction was applied.

The behaviour as a function of the time the signal was sampled and the bias voltage applied was also studied; this is discussed in the two following sub–sections.

5.4.1 Variation with time

The effect was studied as a function of the relative time between the MIP (Minimum Ionising Particle) signal and the sampling time. The TDC time (see Figure 6) was used to divide the data sample into eight 5 ns time windows between -5 ns and 35 ns. Figure 14 shows the relative signal on the neighbouring strips with respect to the central strip for 4 of these time intervals. Only 4 intervals are shown for clarity. The earlier the sampling with respect to the signal, which corresponds to a lower TDC time, a smaller magnitude of the opposite polarity signals is observed in neighbouring strips ±1. By 25 to 35 ns the signal has reached its full deviation.

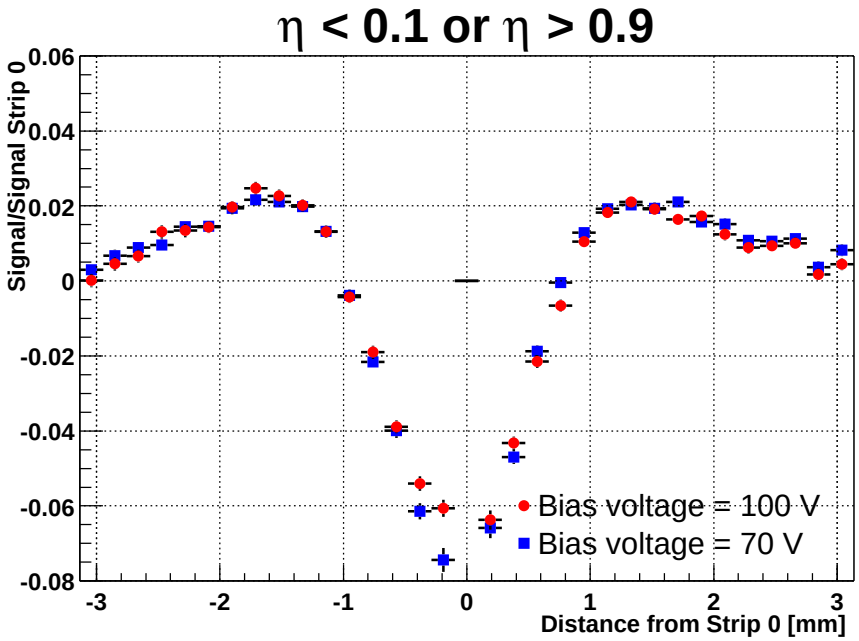

Figure 15: The ratio of signal on ±16 nearest–neighbour strips to that on the strip with a significant positive signal (strip 0) for $\eta < 0.1$ or $\eta > 0.9$, and bias voltages 70 V and 100 V.

5.4.2 Variation with voltage

The data taken with a bias voltage of 70 V were analysed in an identical manner to those taken at 100 V. The η distributions and charge collection were very similar to those for the 100 V sample. Figure 15 shows the relative signal on the neighbouring strips with respect to the central strip for both voltages. The minimum of the negative signals is slightly less for 70 V than 100 V. The minimum relative signal, in the ±1 neighbouring strips, is $\sim -7.5\%$.

5.5 Other measurements of signals in neighbouring strips

This section will examine four different situations where the signal on neighbouring strips has been studied. The measurements are:

- the consecutively bonded strip region of the test detector,
- a narrow pitch n–on–n sensor read out with the SCT128A,
- a wide pitch n–on–n sensor with $\mathcal{O}(1\ \mu\text{s})$ integration time electronics, and
- a wide pitch p–on–n sensor with $\mathcal{O}(25\ \text{ns})$ integration time electronics.

5.5.1 Consecutively bonded strip signals

The region of the detector with consecutively bonded strips was also studied. The sample where no track selection was applied was used to increase the statistics. Figure 16 shows

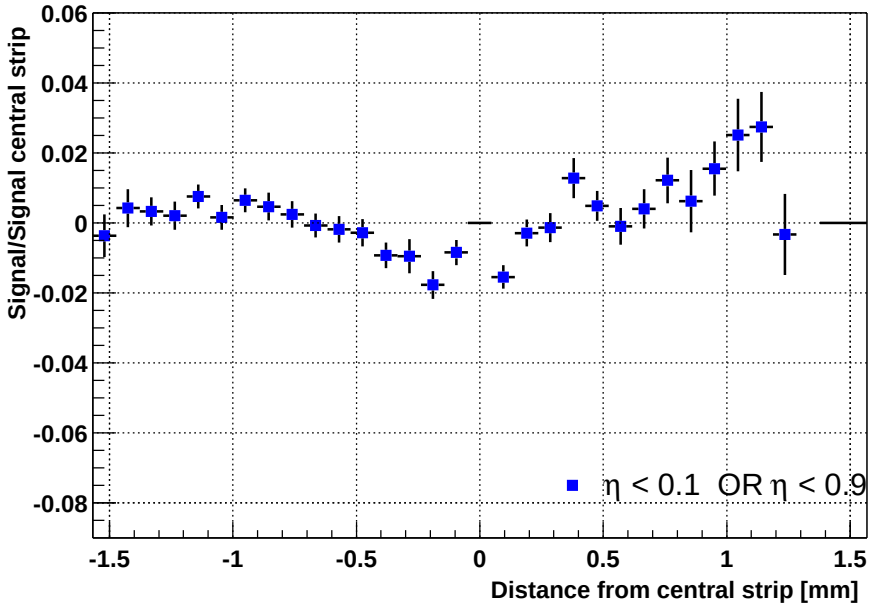

Figure 16: The ratio of signal on ±16 nearest–neighbour strips to that on the strip with a significant positive signal (strip 0) for $\eta < 0.1$ or $\eta > 0.9$. The data used is for a track intercept in the region where strips are bonded consecutively.

the relative signal on the neighbouring strips with respect to the central strip for the $\eta < 0.1$ or $\eta > 0.9$ in this region. Opposite polarity signals can be seen in the strips close to the central strip. The magnitude of the signals is -1% to -2% which is less than that observed in the floating strips region of the detector. Also the signal is asymmetric. There are several possible reasons for this: edge effects, the varying strip length in this region (see Figure 1), the worse alignment in this sample or that only a small number of strips were bonded consecutively

5.5.2 Fine pitch n–on–n detector read out at 40 MHz

Another 300 μm thick n–on–n detector, with pitches of 40 and 60 μm, equipped with SCT128A ASICs was operated in the test–beam. The detector was an R–measuring prototype sensor for the VELO from the PR–01 series manufactured by Hamamatsu.[5] More details of the detector and the electronics can be found in [11].

No opposite polarity signals were observed in the neighbouring strips to a strip with a significant signal. However, it should be noted that in addition to diffusion of the charge within the silicon, there was increased charge sharing between strips within this detector because of its orientation. The beam did not intercept the detector at an angle of $\sim 90°$ as for the test–detector, but at $\sim 80°$, which increases the number of events with significant charge collection on more than one strip.

[5]Hamamatsu Photonics, 325–6, Sunayama–cho, Hamamatsu City, Shizoka Pref., 430–8587, Japan.

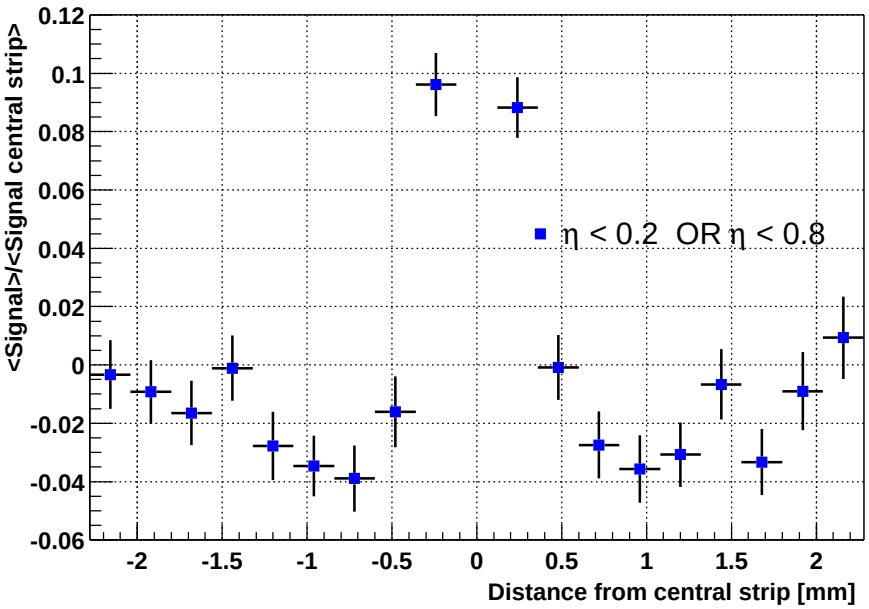

Figure 17: The ratio of the mean signal on ±9 nearest–neighbour strips to the mean signal on a strip with a significant positive signal (strip 0) for $\eta < 0.2$ or $\eta > 0.8$ for a p–on–n detector equipped with the BEETLE ASIC.

5.5.3 $\mathcal{O}(\mu s)$ integration time

The wide pitch region ($\sim 100\mu$m) of the PR–01 ϕ–measuring sensors in the telescope were also studied. The telescope detectors were readout out with the VA2 ASIC [10] which have an integration time of the order 1 μs compared to the 25 ns of the SCT128A. No evidence for opposite polarity signals was found.

5.5.4 Alternative wide pitch detector and 40 MHz electronics

A prototype detector for the LHCb Inner Tracker [14] was also operated in the test–beam in the summer of 2001. The detector had p–on–n strip segmentation, was 300 μm thick and had a strip pitch of 240 μm. The detector was equipped with hybrids carrying the analogue front–end BEETLE ASIC [15], which was operated at 40 MHz. More details of the detector, electronics and measurements can be found in [16] and the references therein.

Figure 17 shows the ratio of the mean signal on the ±9 neighbouring strips to a the mean signal on a central strip for $\eta < 0.2$ or $\eta > 0.8$. For neighbouring strips ±3, ±4 and ±5 there is a significant negative relative signal of between -3% and -4%. The relative signal event–by–event was not significant given the broadening of the distribution due to the low signal–to–noise of ~ 5 for this detector; therefore, the mean values were used.

6 Discussion and conclusions

The conclusions will be divided into two parts, Section 6.1 will contain a discussion of the opposite polarity signals in neighbouring strips to one with a significant signal. Section 6.2 will give general conclusions for the use of floating strips for the VELO's 'ultimate ϕ–measuring sensor'.

6.1 Discussion of opposite polarity signals in neighbouring strips

Section 5.4 reported clear evidence for opposite polarity signals on neighbouring strips to one with a significant signal. The maximum deviations were around -6% to -7%. The signals extend for many strips and and are bi–polar with the signal changing sign further away from the central strip. The bi–polar signals integrate to zero within errors and have a significant extent of $\sim \pm 3$ mm. There is some dependence on sampling time and the bias voltage applied.

Section 5.5 gave examples of other measurements where such signals on neighbouring strips might be observed. Hints of opposite polarity signals were seen in the region of the test detector with consecutively bonded strips. No evidence was found in fine pitch n–on–n detectors read out with 40 MHz electronics, or in wide pitch n–on–n detectors read out with slow, $\mathcal{O}(\mu\text{s})$ integration time, electronics. However, a 240 μm pitch p–on–n detector, read out with fast, $\mathcal{O}(25$ ns) integration time, electronics does indicate some opposite polarity signals in the neighbouring strips.

These observations lead to three conclusions:

- the phenomenon is significant in wide pitch detectors,
- the phenomenon is observed when $\mathcal{O}(25$ ns) integration time electronics are used, and
- the effect is enhanced with floating strips.

Furthermore, the dependence on sampling time and voltage suggests that the signals are induced as the electrons and holes drift towards the implants in the detector's bulk. Opposite polarity signals have been predicted to be induced on neighbouring strips [17] as the charge is being collected; the calculations are performed using Ramo's theorem [18]. However, once all the charge is collected, then these are expected to be cancelled by signals of the same magnitude but different polarity. It should be noted that these simulations were for a pitch of 50 μm only and assume all charge is collected. The 15% deficit in the charge collected in the test detector reported in Section 5.2 could be related to this effect.

To study this effect further a programme of simulation work has begun. This will be reported upon in a subsequent paper.

6.2 Floating strip performance

Sections 5.1 and 5.2 reported on charge sharing and collection for floating strips on a wide pitch n–on–n detector, respectively. The charge sharing was good and the charge

collection on the floating strip was approximately 60% of that on a connected strip. The amount of charge collected on a floating strip could be improved by reducing the ratio between backplane–strip to inter–implant capacitance. It should be noted that the pitch of the 'ultimate ϕ–sensor' design has a maximum of 65 μm [1], compared to the 95 μm strip pitch of the test detector. Therefore, conditions for charge collection are worse in the test–detector than in the 'ultimate ϕ–sensor', due to the reduced inter–strip capacitance in the test–detector. There is no evidence of charge loss in the regions between implants.

The induced negative signals should not be a problem for resolution as the signals of opposite polarity will not be used to form clusters. The negative shift should rarely reduce the signal of a genuine hit because the low occupancy of the VELO sensors of 1% or less [1] means that near neighbouring strips are rarely hit as well. A potential problem is an additional reduction in the signal when the charge is collected on a floating strip, which might become important if the detector has low signal–to–noise.

In conclusion, n–on–n floating strips appear to be viable from the results presented here for charge sharing and efficiency. Opposite polarity signals should not present a problem for the use of floating strips in LHCb. Further R&D is required with respect to radiation hardness and with a strip configuration closer to the 'ultimate ϕ–sensor' design.

7 Acknowledgements

We would like to thank Paul Kuijer from NIKHEF for providing the ALICE detector and information about it. We are indebted to Ian McGill and Kaspar Mühlemann for performing the wire–bonding on the sensor and hybrid. The Inner Tracker Group for the use of their data in Section 5.5.4. We would like to thank Lau Gatignon, Rolf Lindner and the staff of the CERN accelerator division for their support during the test–beam. In addition, we would like to thank the LHCb Test-Beam Data Acquisition Group for the operation and maintenance of the online computing.

References

[1] LHCb collaboration. *LHCb Vertex Locator Technical Design Report.* CERN/LHCC/2001-011.

[2] L. Andricek *et al. Single sided p^+n and double–sided silicon strip detectors exposed to fluences up to $2 \times 10^{14}/\mathrm{cm}^2$ 24 GeV protons.* Nucl. Instr. and Meth. **A409** (1998) 184.

[3] The ALICE Collaboration. *The Inner Tracking System Technical Design Report.* CERN/LHCC/99-12 (1999).

[4] P.P. Allport *et al. FOXFET biassed microstrip detectors.* Nucl. Instr. Meth. **A310** (1991) 155.

[5] F. Aghinolfi *et al. SCTA - a Rad-Hard BiCMOS Analogue Readout ASIC for the ATLAS Semiconductor Tracker.* IEEE Trans. Nucl. Science **44** (1999) 298.

[6] T. Bowcock *et al. Performance of an irradiated n–on–n Hamamatsu prototype VELO detector.* LHCb note, LHCb 2001–039 VELO.

[7] C. Parkes. *Track Fit – Vertex Locator Test–Beam Software Description.* LHCb note, LHCb 2001–038 VELO.

[8] C. Parkes. *Detector Geometry Vertex Locator Test–Beam Software Description.* LHCb note, LHCb 2000–096 VELO.

[9] V. Wright *et al. Study of Resolution of VELO Test–Beam Telescope.* LHCb note, LHCb 2000–103 VELO.

[10] O. Toker *et al. Viking, a CMOS low noise monolithic front–end for Si–strip detector readout.* Nucl. Instr. and Meth. **A340** (1994) 572.

[11] M. Charles *et al. The performance of the SCT128A ASIC when reading out irradiated and non–irradiated VELO prototype detectors.* LHCb note, LHCb 2001–041 VELO.

[12] H. Pernegger. *The Silicon Ministrip Detector of the DELPHI Very Forward Tracker.* PhD thesis, Technischen Universität Wien, (1996).

[13] U. Parzefall. *Private communication.*

[14] O. Steinkamp. *The silicon Inner Tracker for LHCb.* LHCb note, LHCb 2002–009.

[15] N. van Bakel *et al. The Beetle Reference Manual.* LHCb note, LHCb 2001–046 ELEC.

[16] T. Glebe *et al. First Measurements on Inner Tracker Silicon Tracker Prototypes Using The BEETLE v1.1 Readout Chip.* LHCb note, LHCb 2002–018 VELO.

[17] T.J. Brodbeck and A. Chilingarov. *Simulation of charge collection and sharing in microstrip detectors.* Nucl. Instr. and Meth. **A395** (1997) 29.

[18] G. Cavalleri *et al. Extension of Ramo's theorem as applied to induced charge in semiconductor detectors.* Nucl. Instr. and Meth. **A92** (1971) 137.